Available online at www.sciencedirect.com
ScienceDirect
Journal of the European Ceramic Society 31 (2011) 1211–1218
www.elsevier.com/locate/jeurceramsoc

Study of the stability of the molten zone and the stresses induced during the growth of Al_2O_3–$Y_3Al_5O_{12}$ eutectic composite by the laser floating zone technique

D. Sola [a], F.J. Ester [b], P.B. Oliete [a], J.I. Peña [a,*]

[a] *Instituto de Ciencia de Materiales de Aragón, CSIC-University of Zaragoza, c/María de Luna, 3. 50018 Zaragoza, Spain*
[b] *PE3-Laboratorio de Inducción, BSH Electrodomésticos España, S.A.c/Avda. de la Industria 49, 50059 Zaragoza, Spain*

Available online 26 September 2010

Abstract

A series of analytical calculations is used to study both the effect of the thermal gradients and the stability of the molten zone in the laser floating zone growth of Al_2O_3–$Y_3Al_5O_{12}$ eutectic composite. The thermal gradients in the solidification interface have been calculated and the axial gradient compared with the experimental one of 4.5×10^5 K/m. For these calculations the coefficients of heat transfer from the molten zone to the ambient at the solid-melt interface have been previously obtained. The thermal stresses generated by the high thermal gradients can induce crack formation during the cooling depending on the rod diameter. The theory predicts that it is possible to grow rods free of cracks up to $R = 1.7$ mm, at low rates (10 mm/h) in close agreement with the experimental critical radius of 1.6 mm.The dependence of the zone length on the input laser power used to carry out the growth is shown. The study of the floating zone profile allows determining the maximum stable zone length, verifying the stability criterion established by some authors.

Keywords: Al_2O_3; YAG; Thermal shock resistance; Defects; Eutectic

1. Introduction

The laser floating zone technique (LFZ) is a very useful method to explore new materials or to accomplish the high degree of chemical and structural requirements needed for a suitable evaluation of their intrinsic properties. This method of material fabrication encounters its main advantage in inorganic compounds with high melting points or of difficult preparation.[1,2] Initially developed for the high purity silicon growth, it is based on the formation of a small liquid zone, suspended by superficial tension between two solids (precursor and seed) that moves at a controlled speed throughout the precursor producing a directionally solidified rod.

When an infrared laser radiation is used to create the liquid zone, a very high thermal gradient is obtained in the solidification front due to the ability to focus the beam around the precursor. This characteristic allows increasing considerably the speed of crystal growth compared with other methods or heating sources. Moreover, the absence of crucibles minimizes the contamination of the samples. One of the main restrictions of this technique is the geometry of the samples, as they are cylinders with a limitation in the maximum diameter. This maximum diameter depends on the mechanical and thermal properties of the materials and on the thermal gradients at the solidification front. However, the manufacture of ceramic and vitreous materials in fibre form has special interest in several applications as electrical devices (piezoelectric, ferroelectrics, ionic conductors, current leads), optics (laser active fibres, sensors, sapphire light guides) or structural components in which only a low level of defects are allowed in order to achieve the necessary requirements.[3–5]

In this sense, directionally solidified eutectics based in Al_2O_3 (Al_2O_3–Y_2O_3 or Al_2O_3–ZrO_2–Y_2O_3 systems) are of special interest because of the properties derived from the distribution of the phases after solidification (fibres embedded in a matrix, alternate lamellas or non-ordered interpenetrating phases). As a result of these microstructures that depend on the eutectic system and processing conditions, they combine superior flexural strength, toughness, creep resistance at high temperatures and chemical and structural stability up to temperatures close to melting point, making them good candidates to cover the increasing demand

* Corresponding author. Tel.: +34 976761000; fax: +34 976761957.
E-mail address: jipena@unizar.es (J.I. Peña).

0955-2219/$ – see front matter © 2010 Elsevier Ltd. All rights reserved.
doi:10.1016/j.jeurceramsoc.2010.08.022

Table 1
Thermal properties.

	Aluminium oxide[14]		YAG[15]		Air[16]	Al_2O_3/YAG eutectic	
	Solid	Melt	Solid	Melt		Solid	Melt
Density (ρ) (g/cm^3)	3.73	3.053	4.3	3.6	$0.3520/T$	4.04	3.35
Melting temperature (T_m) (K)	2333		2243			2100	
Volumetric expansion coefficient (β) (K^{-1})		2×10^{-4}		1.8×10^{-5}	$1/T$	9.10×10^{-4}	
Thermal conductivity (k) (W/mK)	33 (273 K) 3–6 (HT)	10	8 (2048 K)	4	$1.8 \times 10^{-12}T^3 - 2.33 \times 10^{-8}T^2 + 7.07 \times 10^{-5}T + 2.37 \times 10^{-2}$	7.1 (T = 2048 K)	
Specific heat (C_p) (J/K*kg)	7.96×10^2 (300 K)	1.26×10^3 (2350 K)	8×10^2		$976 + 3.68 \times 10^{-2}T + 1.88 \times 10^{-4}T^2 - 7.11 \times 10^{-8}T^3$	1007	
Latent heat of fusion (ΔH_f) (J/kg)	1.07×10^6		7.07×10^5			1.05×10^6	
Surface tension (σ) (near melting point) (kg/s^2)	$0.7\ \gamma = (\partial\sigma/\partial T) = 6 \times 10^{-5}$ kg/s^2 K		0.78				
Thermal diffusitivity (α) (m^2/s)	1×10^{-6}	2.6×10^{-6}	1.39×10^{-5}		$2.85 \times 10^{-5} + 1.45 \times 10^{-7}T + 4.51 \times 10^{-11}T^2$	7.76×10^{-5}	
Kinematic viscosity (υ) (m^2/s)	8.9×10^{-7}	3.5×10^{-5}	1.28×10^{-5}		$-2.81 \times 10^{-14}T^3 + 1.07 \times 10^{-10}T^2 + 8.80 \times 10^{-8}T + 1.38\text{E}{-}05$	2.28×10^{-5}	
Shear viscosity (μ) (kg/ms)		2.7×10^{-5}	0.046		$2.85 \times 10^{-5} + 1.45 \times 10^{-7}T + 4.51 \times 10^{-11}T^2$	2.65×10^{-2}	
Effective emissivity (ε)	0.78 (300 K) 0.4 (1500 K)		0.3 (solid)			0.345 (1500 K)	

of materials for structural applications at high temperature such as gas turbines or systems for energy generation.[6,7]

In fact, the best mechanical behaviour is obtained for samples that fulfil several requirements such as uniformity in the fibre diameter, structural perfection (free of cracks and pores)[8–10] and compositional homogeneity (without phase segregation)[11,12]. This implies solving a number of problems of zone stability during growth because any deviation will be reflected in defects affecting the quality of the resulting samples. The instabilities may come from laser power fluctuations, non-uniform heat distribution, chamber vibrations, lack of alignment of the rods, excessive zone length, etc.

In this article the conditions of zone stability and temperature distribution during the growth of Al_2O_3–YAG eutectic rods by LFZ are discussed. Relationships between thermal gradients, critical rod diameter and maximum zone length are determined and compared with the predictions obtained from simple analytical calculations.[13] The good correlation observed allows us to consider that this simple model can describe the influence of several growth parameters with the advantage of being practical and quickly applicable to other compounds that produce stable molten zones.

2. Experimental procedure

The precursor rods were obtained from commercial powders of Al_2O_3 (99.99%, Aldrich) and Y_2O_3 (99.99%, Aldrich). The powders were ground in a micromill (model MM2000, Resch, Haan, Germany) with acetone in alumina containers. They were fired in air at 1000 °C, hand milled in an agate mortar to eliminate the agglomerates and mixed in the eutectic composition of $81.5Al_2O_3$–$18.5Y_2O_3$ expressed in % mol. The resulting powder was isostatic pressed at 200 MPa for 2 min obtaining ceramic rods of about 3 mm in diameter and 50 mm long that were sintered at 1500 °C for 12 h.

The laser floating zone system include a CO_2 semisealed laser of 600W (Electronic Engineering, Firenze, Blade600, $\lambda = 10.6$ μm) and an in-house built growth chamber with gold coated metal mirrors for the beam focussing and two vertical axis for the cylinder displacement. Both axes have independent rotation and translation movement. The mirror system inside the chamber consists of a reflaxicon that transforms the solid beam in a ring that is deflected by a flat mirror at 45° and focused in the ceramic rod by a parabolic mirror producing a homogeneous heating. The correct optical alignment is obtained with the aid of a red diode laser coaxial with the infrared beam. The growth process starts heating the lower end of the precursor. Once a drop is formed a small seed placed in the lower axis is approached until a liquid bridge between the precursor and seed is established. Then the seed is moved away at the same time that the precursor is moved to the molten zone maintaining constant the volume of the liquid zone. Identical feed and growth rates were used when equal precursor and eutectic rod diameters are required. To increase or decrease the eutectic rod diameter, the growth rate must be lower or higher respectively than the precursor speed. Neither the precursor nor the rods were rotated. However, a first directional solidification step with counter rotation, previous to the final growth, was generally used to eliminate the porosity of the precursor and to improve the rods alignment.

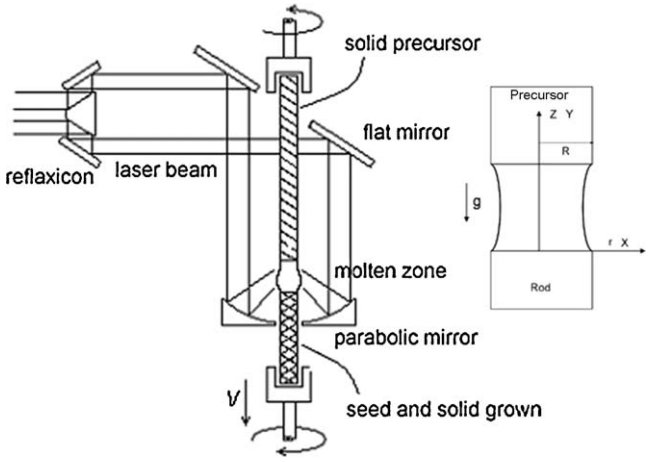

Fig. 1. Experimental layout of the LFZ system for rod growing. Both cylinders move downwards at independent speed. Inside a schematic sketch of the molten zone is shown, Z and r are the axial and radial coordinates, respectively. Y and X are the Cartesian coordinates and R is the radius of the rod.

The images of the molten zone were obtained through a neutral filter with a domestic video camera and a image capture software. A pyrometer (model Minolta/Land Cyclops 52) covering a range between 600 °C and 3000 °C was used to determine the temperature in the liquid and in the growing rod. Laser power was measured with a power meter Synrad PW-250. The microstructure was determined by means of a scanning electron microscope (JEOL JSM6400). Superficial topography and photography were carried out with an optical confocal microscope Nikon Sensofar Plμ2300 and a stereomicroscope.

3. Thermal model

In this section, the temperature profiles and gradients during the growth of the rods are determined and discussed. The thermophysical properties of aluminium oxide, yttrium aluminium garnet and air are given in Table 1. Some data corresponding to the eutectic compound are not known and it has been necessary to use the value obtained by the phase rule from the corresponding ones of aluminium oxide (45 vol.%) and YAG. The microstructure of this eutectic has been described elsewhere.[6,7]

The scheme of LFZ setup and rod growth is shown in Fig. 1. For the calculations, a simplified model of heat transfer from the cylinder is considered. The temperature distribution in the cylinder for the stationary stage is, according to the model of Brice[17]:

$$T(r,z) = T_0 + (T_m - T_0)\frac{1 - hr^2/2R}{1 - 1/2hR}\exp\left[-\left(\frac{2h}{R}\right)^{1/2} z\right] \quad (1)$$

where R is the radius of the cylinder, h is the cooling constant, T_m is the melting temperature of the eutectic (2100 K) and T_0 is the room temperature.

3.1. Heat transfer from the rod

The determination of the cooling rate, h, is necessary for the calculation of the temperature profiles and gradients in the cylinder. It can be obtained from the convection and radiation coefficients. Since the method of calculation has been described previously for Al_2O_3/YSZ eutectic rods[18], only the results will be given here.

$$h_c = \frac{Nu\,k}{D} = \frac{0.1691}{D} \quad (\mathrm{W/m^2K}) \tag{2}$$

where h_c is the convection coefficient, D is the diameter of the rod (in m), Nu is the Nussel Number (2.31) and k the thermal conductivity of the air (Table 1).

Moreover, assuming the molten zone as a grey body with known emissivity, the heat losses by radiation are as follows:

$$q_r = \varepsilon\sigma A_S({T_m}^4 - T_0^4) = h_r A_S(T_m - T_0)$$
$$\text{with} \quad h_r = \varepsilon\sigma(T_m^2 + T_0^2)(T_m + T_0) = 211.2\,\mathrm{W/mK} \tag{3}$$

where $\varepsilon = 0.345$ is an estimation of the Al_2O_3/YAG eutectic emissivity obtained with the ε-values of each separate phase.[19] and σ is the Stefan constant. Then, the total heat transfer coefficient is:

$$h_t = h_r + h_c = 211.2 + \frac{0.1691}{D} \quad (\mathrm{W/m^2K}) \tag{4}$$

h_r is usually higher than h_c and only for rods with small diameters ($D \leq 0.8$ mm) they are comparable.

The cooling constant h is defines as $h = h_t/k$ ($\mathrm{m^{-1}}$), with $k = 7{,}1$ W/mK that was also estimated with the phase rule.

3.2. Axial temperature gradient

The axial gradient in the centre and the surface of the solidification interface ($z = 0$) are defined as follows:

$$\left|\left(\frac{\partial T}{\partial z}\right)_{r=0}\right| = (T_m - T_0)\frac{(2h/R)^{1/2}}{1 - 1/2hR}\ \mathrm{K/m} \tag{5}$$

$$\left|\left(\frac{\partial T}{\partial z}\right)_{r=R}\right| = (T_m - T_0)\left(\frac{2h}{R}\right)^{1/2}\ \mathrm{K/m} \tag{6}$$

3.3. Axial temperature gradient as a function of the growth speed

In the case of a moving rod, the exponential temperature dependence, with a unidimensional model, becomes[18]:

$$\frac{T - T_0}{T_m - T_0} = \exp\left[\left(\frac{1}{2}\right)(Pe - \sqrt{Pe^2 + 8Bi})\frac{z}{R}\right] \tag{7}$$

where $Bi = ((h_r + h_c)R)/k$ is the Biot number, $Pe = (vR)/\alpha$ is the Péclet number, v is the growth speed (in m/s) and α is the thermal diffusivity ($\alpha = 7.76 \times 10^{-5}\ \mathrm{m^2/s}$).

From this equation we can calculate the temperature gradient at $z = 0$ in a rod of radius R.

$$|G_{calc}| = \left|\left(\frac{\partial T}{\partial z}\right)_{Z=0}\right| = \frac{T_m - T_0}{2R}\left[\sqrt{Pe^2 + 8Bi} - Pe\right]\ (\mathrm{K/m}) \tag{8}$$

3.4. Radial temperature gradient

The radial gradient, using Eq. (1), is given by:

$$\frac{\partial T}{\partial r} = -\frac{e^{-z(2(h/R))^{1/2}} hr(T_m - T_0)}{R(1 - (hR/2))} \tag{9}$$

For eutectic rods of Al_2O_3/YAG with radius R, the radial gradient is zero in the centre and in the surface is:

$$\left(\frac{\partial T}{\partial r}\right)_{r=R,z=0} = \frac{(T_m - T_0)h}{R(1 - (hR/2))} = \frac{2080h}{R(1 - (hR/2))}\frac{K}{m} \tag{10}$$

The cracking of the samples during cooling is due to the high radial gradients in the solidification interface. Since the origin of this gradient lies in the heat dissipation from the surface of the cylinder (by radiation and air convection) it can be reduced by an additional heating of the crystal. In this respect, after heaters, lamp heaters, heat reservoirs, gas flow directed towards the melting zone, modification in the laser beam focusing or the use of an atmosphere with greater thermal conductivity than air (for instance, helium) have been used for reducing the thermal gradients.[20,21]

4. Results and discussion

4.1. Thermal gradients

The axial gradient has been measured in the surface of eutectic cylinders near the melt/solid interface with the aid of an optical pyrometer in the steady state. A value of $G_{\mathrm{exp}} = 4.5 \times 10^5$ K/m was obtained for cylinder of 2 mm in diameter. This value is close to the calculated with Eq. (6):

$$\left|\left(\frac{\partial T}{\partial z}\right)_{r=R}\right| = (T_m - T_0)\left(\frac{2h}{R}\right)^{1/2} = 5.2 \times 10^5\ \mathrm{K/m}$$

with the cooling constant for rods of 2 mm in diameter, being

$$h = \frac{h_t}{k} = \frac{84.55 + 211.2}{7.1} = 41.65\ \mathrm{m^{-1}}$$

The axial thermal gradient decreases when the solidification speed of the cylinder increases. In Fig. 2 we represent the calculated temperature gradient for a rod of radius $R = 1$ mm as a function of the growth rate, this dependence is given by:

$$|G_{calc}| = \left|\left(\frac{\partial T}{\partial z}\right)_{Z=0}\right| = \frac{T_m - T_0}{2R}\left[\sqrt{Pe^2 + 8Bi} - Pe\right]$$
$$= \sqrt{1.35 \times 10^{14}v^2 + 2.70 \times 10^{11}} - 1.16 \times 10^7 v(\mathrm{K/m})$$

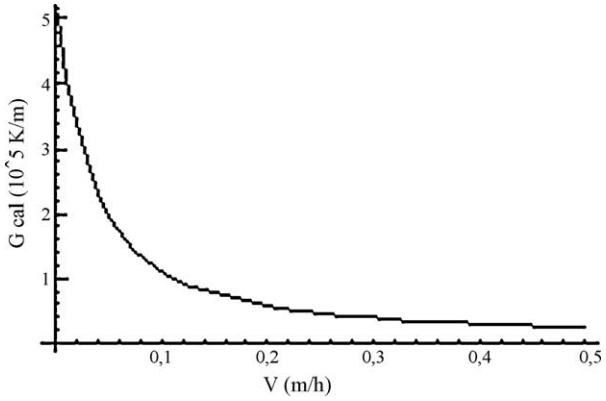

Fig. 2. Representation of the axial thermal gradient as a function of the growth speed for a bar of 2 mm in diameter.

The difference of the temperature calculated in the centre and in the surface of a rod, with $R = 1$ mm, can be obtained from Eq. (1), and is $\Delta T = T_{int} - T_{ext} = 2138 - 2100 = 38\,^{\circ}C$, that serves as an estimation of the radial gradient existing in the solidification interface $(\Delta T/\Delta R)_{R=1\,mm} = 38/(1 \times 10^{-3}) = 3.8 \times 10^4$ K/m.

The calculated radial gradient in the surface of this cylinder is:

$$\left.\frac{\partial T}{\partial r}\right)_{r=R,z=0} = \frac{(T_m - T_0)h}{R(1-(hR/2))} = 7.66 \times 10^4\ \text{K/m}$$

this high gradient at the solidification interface are the cause of the crack formation in thick rods.

4.2. Thermal stresses

One of the effects that limit the thermal gradient with which a cylinder can be grown is the appearance of cracks due to the stresses produced by the temperature differences within the cylinder. If the strain limit (ε_b) is exceeded, the rod is cracked. For these materials it has been considered that ε_b is 4×10^{-4}.[22] In the theory of the elasticity[23], the strain $\varepsilon(R)$ in the surface of a cylinder is:

$$\varepsilon(R) = \frac{\alpha' \Delta T_R}{\sqrt{2}} \tag{11}$$

With an expansion coefficient of $\alpha' = 8.59 \times 10^{-6}\,K^{-1}$ and $\Delta T_R = 38$ K for slow growth rates of rods with $R = 1$ mm, the radial strain of the samples is $\varepsilon(R) = 2.3 \times 10^{-4}$. This value is lower than ε_b, so in these conditions the rod will grow without cracks. The thermal stresses for higher diameters could be high enough to develop the cracking of the sample. However, it is possible to grow rods of higher diameter increasing the growth speed because the thermal gradients are reduced as we have discussed in Section 3.3.

In fact, rods with different diameters between 1.0 and 4.0 mm have been grown at a growth speed of 10 mm/h with cracks being detected for $R > 1.6$ mm (Fig. 3a). However, for refractory materials these diameters are in the limit of the LFZ technique because the melting of the centre of the rod is hardly achieved even at the slowest speeds. Fig. 3a shows the image of a cracked sample of $R = 1.6$ mm taken with a stereomicroscope. Problems with rod cracking during growth at slow solidification rates (10 mm/h) were only experienced with Al_2O_3/YAG rods over $R = 1.6$ mm and with Al_2O_3/ZrO_2 ($3Y_2O_3$) rods over $R = 0.6$ mm (20). Fig. 3b and c shows the topographic images of the surfaces of these rods when the radius exceeds the critical one.

This critical radius can also be predicted for a determined solidification rate comparing the thermal gradient in the rod and the calculated critical gradient as a function of the radius.

From Eqs. (9) and (6) ΔT_R can be written as:

$$\Delta T_R = \frac{R}{2}\left(\frac{hR}{2}\right)^{1/2}\frac{dT}{dz}\left(1-\frac{hR}{2}\right)^{-1} \tag{12}$$

And $\varepsilon(R)$ takes the form:

$$\varepsilon(R) = \frac{\alpha}{\sqrt{2}}\frac{R}{2}\left(\frac{hR}{2}\right)^{1/2}\frac{dT}{dz}\left(1-\frac{hR}{2}\right)^{-1} \tag{13}$$

Then, the maximum axial gradient is given by:

$$G_{crit} = \left.\frac{dT}{dz}\right|_{max} = \frac{2\varepsilon_b\sqrt{2}}{R\alpha}\left(\frac{hR}{2}\right)^{-1/2}\left(1-\frac{hR}{2}\right) = \frac{28.86}{R^{3/2}}(1-20.82R) \tag{14}$$

On the other hand, the expression of the axial gradient as a function of the radius can be derived from [7]. With a solidification speed $v = 10$ mm/h $= 2.78 \times 10^{-6}$ m/s it is:

$$G_{calc} = \frac{\partial T}{\partial z} = -\frac{T_m - T_0}{2R}\left[\sqrt{Pe^2 + 8Bi} - Pe\right] = \frac{1835}{2R}\left[\sqrt{8.53R^2 + 594.2R} - 2.92R\right] \tag{15}$$

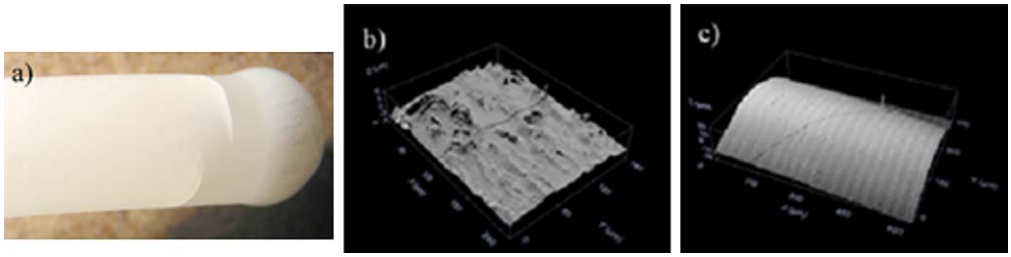

Fig. 3. (a) Stereoscopic image of a cracked Al_2O_3/YAG rod, (b) and (c) topographic image of the surface of Al_2O_3/YAG and Al_2O_3/ZrO_3 ($3Y_2O_3$), respectively, grown at 10 mm/h.

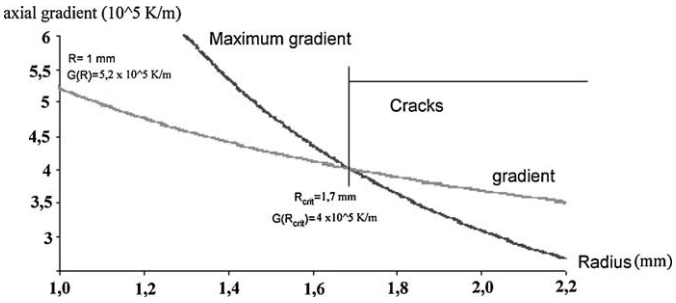

Fig. 4. Calculated critical and axial temperature gradients as a function of the rod radius. The intersection establishes the critical radius below which the rods grow free of cracks.

Both gradients are represented in Fig. 4b. Whereas the axial gradient during the growth stays below the critical one the rods will grow without cracks. Therefore, the intersection of both curves represent the critical radius, $R_{crit} = 1.7 \times 10^{-3}$ m, corresponding to a gradient of $G(R_{crit}) = 4 \times 10^5$ K/m.

This representation has been done for a growth speed of 10 mm/h that is considered a slow speed of solidification. In these conditions the samples present a homogenous microstructure formed by phases of alumina and YAG finely dispersed and interpenetrated.[24] At higher speeds the interpenetrated network remains but the size of the phases is smaller and, as a consequence, the mechanical behaviour of the samples is better.[25] However, if we want to assure the whole melting of the rods, when high growth rates are used they cannot be too thick. The short penetration of the heat towards the interior can prevent the formation of a totally liquid zone, remaining the interior as a solid nucleus. For example at 500 mm/h the rods should not be thicker than 1 mm in diameter.

As a conclusion it is possible to say that the higher the growth speed is, the lower the axial gradient. Lower axial gradients allow the growth of thick cylinders without cracks. In the case of Al_2O_3/YAG eutectics, the size of the samples is not a problem because it is possible to grow thick rods even at slow speeds. But in the case of the Al_2O_3/ZrO_2 (Y_2O_3), rods of $R = 1$ mm can be grown without cracks only at moderate solidification speed (above 100 mm/h).[26]

4.3. Molten zone shape

The stability of the melting zone depends on the shape (length to diameter relationship), on material properties (surface tension of the melt, melting temperature) and on some external conditions (atmosphere pressure, and presence of gravity). If the liquid zone is not stable some defects related to composition inhomogenities and lack of uniformity in the rod diameter appear, even the separation of the liquid zone into two drops if the length surpasses the maximum.

The analysis of the shape and stability of a floating zone was done by Saitou[27]. Ester and Peña[18] applied this analysis to the study of the eutectic Al_2O_3/ZrO_2 (Y_2O_3). They demonstrated their utility to obtain important growth parameters, as the stability range (maximum zone length), or thermophysical properties usually not found in the literature, as the surface tension. The

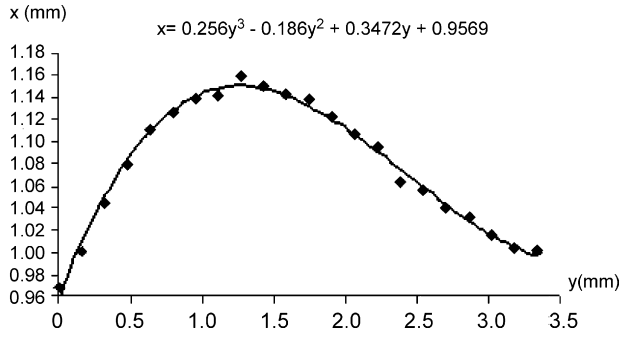

Fig. 5. Curve of the surface shape corresponding to the left side of the floating liquid zone. The dots are the experimental points corresponding to the radial positions of the melt/air interface at various axial positions. The solid line denotes the simulation result.

equation that represents the profile of the floating zone is[27]:

$$x = \frac{y^3}{6C^2} + \frac{\lambda y^2}{2C} + C_0 y + C_1 C \tag{16}$$

The parameters C, λ, $C_0 y$ and C_1 can be obtained adjusting this equation to an experimental profile. In our case we have used the zone corresponding to a rod of 0.89 mm in radius, grown at 10 mm/h with a laser power of 102 W (Fig. 5). Fig. 5 represents the experimental left profile of this zone (dots) and the curve obtained adjusting Eq. (17) to these experimental points. X is the distance to the rod axis as a function of the height (Y).

C_0 is related to the length of the liquid zone, h, through the expression:

$$C_0 = \frac{l^2}{12C^2} + 6(n-1)\frac{R}{h} \tag{17}$$

with n a positive real number.

$C_0 = 0.3472$ gives $n = 1.099$, when n is greater than one the shape of the floating zone is convex to the exterior.

The upper limit for the molten zone, according to the equations given by Saitou, is:

$$R < h\frac{(1 - h^2/12C^2)}{6|n-1|} \quad \text{if } C_0 < 1 \text{ and } n > 1. \tag{18}$$

In Fig. 6 the points under the curve represent the zone of growth stability. For a rod with $R = 0.89$ mm, two limit values of zone length are defined, $h_{min} = 0.41$ mm and $h_{max} = 7.84$ mm, that cor-

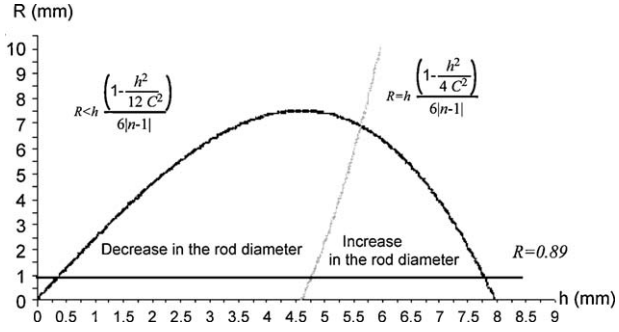

Fig. 6. Stability diagram for the floating liquid zone. The radius of the rod is 0.89 mm. The left part represents the stable conditions with decrease in the width of the grown rod, the right part with increase in the width of the grown rod.

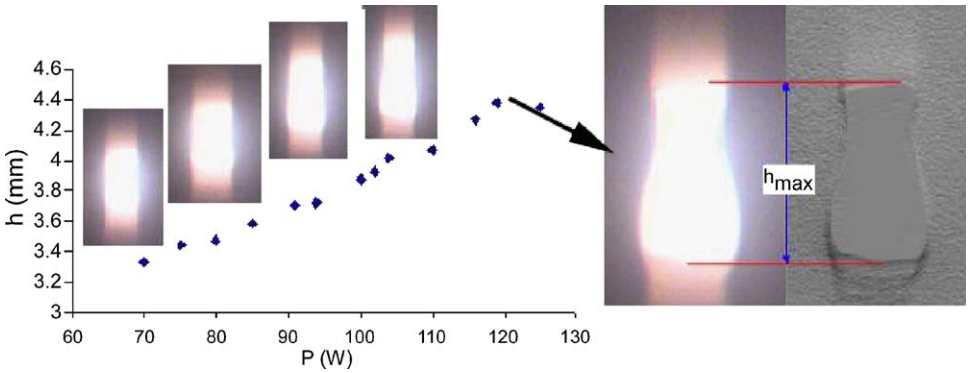

Fig. 7. Molten zone lengths (h) at various laser power (P) with images of the molten zones for some input power captured experimentally.

respond to the zone length at which the rod grows with the maximum reduction or increase in its diameter. However there is another additional condition that separates both zones:

$$R = h\frac{(1-(h^2/4C^2))}{6|n-1|} \tag{19}$$

This curve corresponds to the stability condition when the rod grows without change in the diameter and the intersection with the horizontal line defines the maximum length of the zone when the rod grows with the same diameter than the precursor. In this case, $h_{max} = 4.81$ mm.

We have grown rods trying to verify the validity of this theory, and the maximum lengths of the zone measured are 0.75, 5.14 and 4.4 mm when the diameter of the rod decreases, increases or remains equal to the precursor, respectively.

Fig. 7 shows the evolution of the zone length with the laser power, from the minimum power required for producing a molten zone to the separation of the zone in two hemispheres. The float zone falls out when the length exceeds 4.4 mm, slightly lower than the critical length predicted by the theory.

Heywang[28] gave an expression to determine the maximum stable zone length, $h_{max} = 2.84(\sigma/\rho g)^{1/2}$, for a zone radius sufficiently large. Applying this equation to our case, the length obtained is $h_{max} = 4.62$ mm, very similar to the experimental one as well as the predicted by Saitou.

On the other hand, Pfann and Hagelbarger[29] have shown that in a zero-gravity environment the zone remains stable while the length does not exceed its circumference (Rayleigh limit), $h_{max} = \pi \times D$. In the case of a rod of $R = 1$ mm, the equation gives a h_{max} of 5.59 mm, which is higher than the one predicted by Saitou, maybe because the expression of Pfann does not consider the effect of the gravity. Then, this simplified relationship between zone length and diameter could be applied only to thin rods, where the weight of the melt is not too important, or in zero-gravity conditions. Coriell et al.[30] also showed that the maximum zone length depends on the radius and decreases with an increase in the strength of the gravity.

5. Conclusions

A method to analyse the stability conditions during the process of laser floating zone of Al_2O_3–YAG eutectic rods has been described. The coefficients of heat transfer and temperature distribution in the solid during growth have been calculated and compared with the experimental thermal gradient in the melt-solid interface, obtaining a good agreement. It is possible to grow rods free of cracks if the diameter does not exceed a critical one established in 3.4 mm for growth rates of 10 mm/h. Rods with higher diameters can be grown increasing the speed of solidification due to the reduction in the axial gradient. From the analysis of the profile of the liquid zone, the maximum stable zone length has been determined and compared with the experimental, showing a good correlation with the predictions by some authors.

Acknowledgements

This work was supported by the European Union through the project ENSEMBLE NMP4-2008-213669 and Spanish Ministry of Science and Innovation (MAT2009-13979-C03-03). F.J. Ester and D. Sola gratefully acknowledge BSH Electrodomésticos España, S.A. for their contracts.

References

1. Feigelson RS. Pulling optical fibers. *J Cryst Growth* 1986;**79**:669–80.
2. Peña JI, Merino RI, Harlan NR, Larrea A, de la Fuente GF, Orera VM. Microstructure of Y_2O_3 doped Al_2O_3–ZrO_2 eutectics grown by the laser floating zone method. *J Eur Ceram Soc* 2002;**22**:2595–602.
3. Angurel LA, Diez JC, Martínez E, Peña JI, de la Fuente GF, Navarro R. Growth rate effects on thin $Bi_2Sr_2CaCu_2O_{8+\delta}$ textured rods. *Physica C* 1998;**302**:39–50.
4. Luh YS, Feigelson RB, Fejer MM, Byer RL. Ferroelectric domain structures in $LiNbO_3$ single crystal fiber. *J Cryst Growth* 1986;**78**:135–43.
5. Nubling RK, Harrington JA. Optical properties of single-crystal sapphire fibres. *Appl Optics* 1997;**36**:5934–40.
6. Merino RI, Peña JI, Larrea A, de la Fuente GF, Orera VM. Melt grown composite ceramics obtained by directional solidification: structural and functional applications. *Recent Res Dev Mater Sci* 2003;**4**:1–24.
7. Llorca J, Orera VM. Directionally solidified eutectic ceramic oxides. *Progr Mater Sci* 2006;**51**:711–809.
8. Oliete PB, Peña JI. Study of the gas inclusions in $Al_2O_3/Y_3Al_5O_{12}$ and $Al_2O_3/Y_3Al_5O_{12}/ZrO_2$ eutectic fibres grown by laser floating zone. *J Cryst Growth* 2007;**304**:514–9.
9. Peña JI, Larsson M, Merino RI, de Francisco I, Orera VM, Llorca J, et al. Processing, microstructure and mechanical properties of directionally-solidified Al_2O_3–$Y_3Al_5O_{12}$–ZrO_2 ternary eutectics. *J Eur Ceram Soc* 2006;**26**:3113–21.

10. Saito M. Growth process of gas bubble in ruby single crystals by floating zone method. *J Cryst Growth* 1986;**74**:385–90.
11. Lim HJ, DeMattei RC, Feigelson RS, Rochford K. Striations in YIG fibers grown by the laser heated pedestal method. *J Cryst Growth* 2000;**212**:191–203.
12. de Francisco I, Merino RI, Orera VM, Larrea A, Peña JI. Growth of $Al_2O_3/ZrO_2(Y_2O_3)$ eutectic rods by the laser floating zone technique: effect of the rotation. *J Eur Ceram Soc* 2005;**25**: 1341–50.
13. Kuo VHS, Wilkox WR. Influence of crystal dimensions on the interfacial temperature gradient. *J Cryst Growth* 1972;**12**:191–4.
14. Kirshenbaum AD, Cahill JA. The density of liquid aluminium oxide. *J Inorg Nucl Chem* 1960;**14**:283–7.
15. Galazka Z, Wilke H. Heat transfer and fluid flow Turing growth of $Y_3Al_5O_{12}$ single crystals using Czochralski method. *Cryst Res Technol* 2000;**35**:1263–78.
16. Kreith F, Chapman AJ. *Heat transfer*. 4th ed. New York: McMillan; 1984. p. 556.
17. Brice JC. Analysis of the temperature distribution in pulled crystals. *J Cryst Growth* 1968;**2**:395–401.
18. Ester FJ, Peña JI. Análisis de la zona fundida en el crecimiento del compuesto eutéctico Al_2O_3–ZrO_2 (Y_2O_3) por fusión zonal con láser. *Bol Soc Esp Ceram V* 2007;**46**:240–6.
19. Sully AH, Brades EA, Waterhouse RB. Some measurement of the total emissivity of metals and pure refractory oxides and the variation of emissivity with temperature. *Brit J Appl Phys* 1952;**3**:97–101.
20. Reyes Ardila D, Barbosa LB, Andreeta JP. Bifocal spherical mirror for laser processing. *Rev Sci Instrum* 2001;**72**:4415–8.
21. Tong L. Growth of high-quality Y_2O_3–ZrO_2 single-crystal optical fibers for ultra-high-temperature fiber-optic sensors. *J Cryst Growth* 2000;**217**:281–6.
22. Pastor JY, Poza P, Llorca J, Peña JI, Merino RI, Orera VM. Mechanical properties of directionally solidified Al_2O_3–ZrO_2 (Y_2O_3) eutectics. *Mater Sci Eng A* 2001;**308**:241–9.
23. Timoshenko SP, Goodier JN. *Theory of elasticity*. McGraw-Hill; 1970.
24. Nakagawa N, Ohtsubo H, Mitani A, Shimizu K, Waku Y. High temperature strength and thermal stability for melt growth composite. *J Eur Ceram Soc* 2005;**25**:1251–7.
25. Pastor JY, Llorca J, Salazar A, Peña JI, de Francisco I, Oliete PB. Mechanical properties of melt-grown alumina–YAG eutectics up to 1900 K. *J Am Ceram Soc* 2005;**88**:1488–95.
26. Ester FJ, Sola D, Peña JI. Efectos térmicos inducidos durante el crecimiento del compuesto eutéctico Al_2O_3–$ZrO_2(Y_2O_3)$ por fusión zonal con láser. *Bol Soc Esp Ceram V* 2008;**47**:7–12.
27. Saitou M. Shape and stability of a floating liquid zone between two solids. *J Appl Phys* 1997;**82**:6343–5.
28. Heywang W. Zur stabilitat senkrechter smelzzonen. *Z Naturforsch Part A* 1956;**11**:238–43.
29. Pfann WG, Hagelbarger DW. Electromagnetic suspension of a molten zone. *J Appl Phys* 1956;**27**:12–8.
30. Coriell SR, Hardy SC, Coprdes MR. Stability of liquids zones. *J Colloid Interface Sci* 1977;**60**:126–36.